THE JOURNAL OF COMPARATIVE NEUROLOGY 438:490–504 (2001)

Short and Mid-Wavelength Cone Distribution in a Nocturnal Strepsirrhine Primate (*Microcebus murinus*)

OURIA DKHISSI-BENYAHYA,[1] AGOSTON SZEL,[2] WILLEM J. DEGRIP,[3] AND HOWARD M. COOPER[1]*

[1]I.N.S.E.R.M. Unité 371, Cerveau et Vision, 69675 Bron, France
[2]Department of Human Morphology, Semmelweis University, H-1094 Budapest, Hungary
[3]Department of Biochemistry UMC-160, Nijmegen Centre of Molecular Life Sciences, University of Nijmegen, Nijmegen 6500 HD, The Netherlands

ABSTRACT

Strepsirrhines are of considerable interest for understanding the evolution of cone photoreceptors because they represent the most ancestral living primates. The retina of nocturnal Strepsirrhines is reported to contain a single population of medium/long wavelength (MW/LW) cones whereas short wavelength (SW) cones are totally absent. The area centralis of nocturnal Strepsirrhines also lacks the degree of central specialization seen in the fovea of diurnal primates. In this study of a nocturnal Strepsirrhine, the gray mouse lemur (*Microcebus murinus*), we used specific antibodies that recognize SW and MW/LW opsins to determine the presence of different cone subtypes and their distribution in relation to that of rods and ganglion cells. The results are compared to two diurnal Haplorhine species, a New World (*Callithrix jacchus*) and an Old World (*Macaca fascicularis*) monkey. In the mouse lemur, both antibodies to MW/LW cone opsin (COS-1 and CERN956) label the same population of cones. A small proportion of SW cones is only stained by the JH455 antiserum whereas the monoclonal OS-2 antibody shows negative staining. These two antibodies label the same SW cone population in other primates. The extracellular matrix of all cones is also labeled by the peanut agglutinin (PNA) lectin. In mouse lemur retinal wholemounts, peak cone density is localized at the area centralis and ranged from 7,500 to 8,000 cones/mm^2. SW cones represent less than 0.2 % of the total cone population and are mainly located in the nasal part of the retina. SW cones show an irregular distribution and densities never exceed 49 cones/mm^2. The distribution of neurons in the ganglion cell layer shows a distinct centroperipheral gradient with a peak of 28,000 cells/mm^2 at the area centralis. Rod distribution shows a centroperipheral gradient with the peak (850,000 rods/mm^2) including and extending slightly dorsal to the area centralis. The theoretical spatial resolution of the mouse lemur (4.9 cycles/degree) is slightly lower to that of other nocturnal primates. The densities of rods, cones, and ganglion cell layer neurons represent a compromise between spatial resolution and sensitivity for both photopic and scotopic vision. J. Comp. Neurol. 438: 490–504, 2001. © 2001 Wiley-Liss, Inc.

Indexing terms: photoreceptors; opsin; ganglion cells; retina; rods; prosimian

Opsin is a major membrane protein of the photoreceptor outer segment that combines with photosensitive 11-*cis* retinal to form the cone and rod visual pigments. All mammals possess duplex retinae with rods and at least one type of cone photoreceptor. Cone photoreceptors are divided into three functional types according to spectral sensitivity: short (SW), medium (MW), or long (LW) wavelength sensitive. Interactions between these different cone types are essential for color vision.

In most mammals, the color vision system is dichromatic and depends on the presence of two types of cone photoreceptors with peak spectral sensitivity in the MW (500–530 nm, sensitive to green light) and SW-sensitive

Grant sponsor: Human Frontiers; Grant number: RG95/68; Grant Sponsor: Biomed2; Grant number: BMH4-CT972327; Grant sponsor: INSERM Est-West; Grant Sponsor: Hungarian OTKA-Fund; Grant number: T29048.

*Correspondence to: Dr. Howard. M. Cooper, Unité 371, 18 Avenue du Doyen Lépine, 69675 Bron, France. E-mail: cooper@lyon151.inserm.fr

Received 26 December 2000; Revised 31 May 2001; Accepted 5 July 2001

© 2001 WILEY-LISS, INC.

range (near 430 nm, sensitive to blue or near ultraviolet depending on the species; Bowmaker et al., 1991; Jacobs, 1993, 1996). Structural comparisons of cone opsin genes show that a divergence in cone opsins first occurred between SW and MW photopigments (Yokoyama and Yokoyama, 1989), providing the basis for dichromatic color vision. The divergence from MW to LW cone pigments from the MW/LW cone ancestor is a more recent event in the evolutionary history of primates (Yokoyama and Yokoyama, 1989; Hunt et al., 1995; Jacobs et al., 1996a). Diurnal primates are thus unique among mammals to possess trichromatic color vision (reviews: Nathans et al., 1986; Jacobs et al., 1993), a capacity that appears to have evolved in relation to foraging behavior and fruit with characteristic color cues (Cooper et al., 1986; Lythgoe and Partridge, 1989; Regan et al., 1998).

Exceptions to the rule of dichromacy in mammals have been reported in the last few years because species of several orders have been shown to lack SW pigment expression. An absence of SW cones has been found in nocturnal rodents and carnivores: the pygmy field mouse and Gairdner's shrew mouse (Szel et al., 1996), the Syrian golden hamster (von Schantz et al., 1997; Calderone and Jacobs, 1999), the raccoon, Kinkajou (Jacobs and Deegan, 1992), in seals, as well as in Cetaceans (Fasick et al., 1998). Although most other nocturnal species possess both SW and MW cones, these observations suggest that the absence of SW cones is restricted to mammals in the nocturnal environment or, in the case of Cetaceans, to conditions of low visibility or turbidity in water (for review, see Ahnelt and Kolb, 2000; Peichl et al., 2001).

Although the majority of primates are diurnal, exceptions include most Strepsirrhines and a single species of New World primates (*Aotus trivirgatus*) which are nocturnal. Indeed, the absence of SW cones was first reported for two nocturnal primate species, the owl monkey (*A. trivirgatus*) and the greater bushbaby (*Galago garnetti*; Wikler and Rakic, 1990). These authors found no SW cone opsin immunoreactivity in these species and electrophysiological recordings support this finding (Jacobs et al., 1993). Jacobs et al. (1996b) have shown subsequently that although an SW cone opsin gene is present in these two species, the protein is not expressed because of deleterious mutational changes in the amino acid sequence. However, two diurnal lemurs (*Eulemur fulvus* and *Lemur catta*) have been shown to possess MW/LW and SW cone pigments (Jacobs and Deegan, 1993).

These observations would appear to support the idea that the absence of SW cone opsin in these primates is related to nocturnal behavior, particularly in the case of *Aotus*, which descends from diurnal ancestors. However, the presence of SW cones has been reported recently in Tarsius, a nocturnal primate that also belongs to the haplorhine primate lineage (Hendrickson et al., 2000). Furthermore, a recent study in seals, which are visually active both during day and night, argues that the absence of SW cones is not exclusively associated with nocturnality (Peichl and Moutairou, 1998).

It has been suggested that the early primates were nocturnal (Kay and Kirk, 2000). Therefore, Strepsirrhines and Tarsius are of significant interest because they represent the most ancestral living primates and possess many anatomical and behavioral characteristics of ancestors that are also common to present-day monkeys, apes, and humans (Blakeslee and Jacobs, 1985; Kay et al.,1997). The study of cone opsins and their distributions in these primates is relevant to an understanding of the evolution of primate color vision and the fovea. Our knowledge of color vision in nocturnal primates is fragmentary (Dartnall et al., 1965; Casagrande and DeBruyn, 1982). Trichromacy in Human, New, and Old World monkeys is due to an SW opsin gene localized in an autosomal chromosome and to MW/LW opsin genes on the X chromosome. Thus, polymorphisms at the X-linked locus can lead to trichromacy in heterozygous females although males and homozygous females are dichromatic (Martin and Grünert, 1999). In contrast, nocturnal Strepsirrhines are monochromatic due to a mutation in the SW opsin gene (Deegan and Jacobs, 1996). A recent report in 20 Strepsirrhines found a polymorphism at the X-linked locus in two species of the two major diurnal lineages but only one nocturnal species (*Greater dwarf lemur*) shows this polymorphism (Tan and Li, 1999).

In the present study, we aim first to determine whether all cone subtypes and specifically the SW cone opsin are present in a nocturnal Strepsirrhine species (*Microcebus murinus*). Second, we describe the morphological characteristics of cone photoreceptors. Finally, we analyze the distribution of cones in relation to that of rods and ganglion cell layer neurons. The results are compared with two diurnal species from other major primate groups: a New World (*Callithrix jacchus*) and an Old World (*Macaca fascicularis*) monkey.

MATERIALS AND METHODS

Tissue collection and preparation

Eleven retinas from eight adult gray mouse lemurs (*M. murinus*), one eye of a marmoset (*C. jacchus*), and one of a macaque (*M. fascicularis*) were used in this study. The mouse lemurs were obtained from the Laboratory of General Ecology (Brunoy, France), where the breeding colony (licence approval number A91.114.1) had been established from wild animals originating from Southwest Madagascar 30 years ago. The other primates were part of the colony in INSERM (licence number B 69-685). All animals were maintained and treated according to current national and international standards.

Animals were anesthetized deeply with ketamine (150 mg/kg intraperitoneally [i.p.]) followed by an i.p. injection of nembutal (100 mg/kg i.p.). They were then perfused intracardially with warm (37°C) heparinized saline followed by Zamboni's fixative at 4°C. The eyes were removed from the skull, opened, and postfixed overnight in the same fixative at 4°C and subsequently stored in 0.1 M phosphate buffer (PB; pH 7.4) with 0.1% sodium azide. For wholemounts, the eye was marked for orientation while still in place in the orbit. Retinas were dissected free from the sclera and the pigment epithelium and the vitreous was cleaned away. The free-floating retinas were stored in PB with 0.1% sodium azide at 4° C until use. To obtain retinal sections, entire eyes were cryoprotected in 30% sucrose in PB (pH 7.4) for 24 hours. Serial sections of the retina were made at 15 μm on a freezing microtome. Free-floating retinas and retinal sections were processed identically for immunohistochemistry.

Immunohistochemistry

Antibodies. To identify cone photoreceptors in retinal sections and wholemount retinas, we used the biotinyl-

ated lectin peanut agglutinin (PNA-b, Vector Laboratories, Burlingame, CA), which binds to the extracellular matrix of all cones. The SW cone opsin was detected by using two antibodies, the affinity-purified rabbit antisera JH455 (1/5,000) directed against the human SW cone opsin (gift provided by Dr. J. Nathans; Wang et al., 1992) and the mouse monoclonal antibody OS-2 (1/2,500) produced against chicken photoreceptor membranes (Szel et al., 1986). The MW/LW cone opsin was detected with the mouse monoclonal antibody COS-1 (1/100) generated to chick opsins (Szel et al., 1986) and the polyclonal antibody CERN956 (1/1,000) directed against the human MW/LW opsin (Vissers and DeGrip, 1996).

Multiple labeling was performed in the different species in retinal sections and/or wholemounts. Combinations of antibodies were used according to the tissue preparation (free-floating sections or wholemount retina), the antibodies, or the technique of visualization (immunoperoxidase or immunofluorescence).

Typically, free-floating sections were preincubated in phosphate-buffered saline (PBS; 0.01 M, pH 7.2) containing 0.3% triton and 0.1% sodium azide (PBSTA) with 1% bovine serum albumin (BSA) to block nonspecific binding sites. Retinal sections were then incubated in a single antibody or in two mixtures of antibodies for SW and MW/LW opsins: (1) COS-1 and JH455 and (2) OS-2 and JH455. After 4 days of incubation at 4°C, the binding sites of the primary antibodies were visualized in a mixture of secondary antisera, i.e., goat anti-rabbit Alexa 568 IgG (H+L) conjugate (100 μg/ml, Molecular Probes, Eugene, OR) and goat anti-mouse Alexa 488 IgG (H+L) conjugate (100 μg/ml, Molecular Probes) for 2 hours. In some cases, sections were then washed twice in PBST and incubated at room temperature for 2 hours in PNA-b (100 μg/ml), which was revealed by using AMCA avidin D (100 μg/ml, Vector Laboratories).

Wholemount immunocytochemistry

Wholemount immunocytochemistry was done according to the above procedure with the following changes. Endogenous peroxidase was first suppressed by using a solution of 50% absolute alcohol in saline with 0.03% H_2O_2. Retinas were rinsed in PBSTA (0.01 M, pH 7.2) containing 0.3% Triton X-100 and 0.1% sodium azide and blocked with 1% BSA and then incubated either with COS-1 or JH455 for 4 days at 4°C on a shaker, washed twice in PBST, and then reacted in the secondary species-specific biotinylated IgG (1/200) for 2 hours at room temperature. After these steps, different procedures were followed. (1) Immunoreactivity was visualized by using a Vectastain ABC Elite kit (PK-6100, Vector Laboratories), followed by incubation in 0.2% 3,3'-diaminobenzidine (DAB) with 0.5% ammonium nickel sulfate and 0.003% H_2O_2 in Tris buffer (TRIS 0.05 M, pH 7.6). Retinas were washed twice in TRIS followed by one rinse in PBST. An avidin-biotin blocking kit (Vector Laboratories) was used to block nonspecific binding of biotin/avidin reagents. Retinas were incubated with avidin D blocking solution for 30 minutes, rinsed twice in PBST, and incubated overnight with the biotin blocking solution. These steps were performed prior to the addition of the PNA-b (2 hours, room temperature). PNA-b reactivity was visualized by the Texas Red avidin D (50 μg/ml, 2 hours, Vector Laboratories). (2) Immunoreactivities were visualized by using the Texas Red avidin D (50 μg/ml, 2 hours, Vector Laboratories), followed by the PNA-FITC conjugate (100 μg/ml, 2 hours), and anti-FITC (100 μg/ml, 2 hours) to amplify PNA labeling. Retinal sections and wholemount retinas were coverslipped, photoreceptor side up (for wholemounted retinas) in adequate mounting medium. This procedure allowed staining of all cones (PNA) in addition to a specific cone type (SW or MW/LW). Controls were made by omitting the primary antibody or by replacing it with normal serum at the same concentration as the antibody. No labeling was observed in control sections.

Count of ganglion cell layer neurons

After photoreceptor counts, one wholemounted retina was removed from the slide, placed cell layer up, and counterstained with cresyl violet. The number and distribution of cells in the ganglion cell layer was counted by using the plotting system described in the following paragraph. These counts include both ganglion and displaced amacrine cells.

Plotting system and image processing

The location of fluorescent or immunoperoxidase-labeled cone photoreceptors in wholemounts was plotted by means of a computerized semiautomatic plotting system developed in the laboratory. The system included a Leitz microscope equipped with a motorized XY stage. A digitized pad enabled precise displacement of the XY stage. An interface from the stage to the computer allowed recording of the XY coordinates of the position of labeled cells. A complete map of the flattened retina was drawn. In 70–90 sample fields across the retina, cones and neurons in the ganglion cell layer were counted by the observer with a 50× oil immersion objective and the data recorded by the computer system. Samples were made at an interval of every 1–1.2 mm. Data stored in files could then be used for cell counts, cell densities, and printouts of photoreceptor isodensity maps. Cell densities across the retina were calculated from the recorded samples by using an automated system based on a two-dimensional spline surface interpolation algorithm. The algorithm is capable of automatically tracing isodensity contours of the retinal map from the data files.

The plotting system was impractical to use directly from rod counts considering the high density and small size of rod photoreceptors. To be able to count rods in the same area as the cones and the ganglion cell layer neurons, a well-defined area was chosen and photographed by using differential interference contrast (DIC). In each print, a 20 × 20-μm square was outlined and rods within the square were counted. Each count (rods/mm^2) was recorded on the retinal map by using the plotting system described above, which allowed calculation of the isodensity maps of rods, cones, and ganglion cell layer neurons from the same retina.

For image processing, fluorescent multiple-labeled cells were digitized by using a cooled color digital camera (Spot II, Diagnostic Instruments, Sterling Heights, MI) on a Leica DMR fluorescence microscope. Adobe Photoshop software was used for image treatment.

RESULTS

Retinal photoreceptors in flatmount

The mouse lemur has a relatively large eye measuring 9.65 mm in diameter (anteroposterior axis). Observation

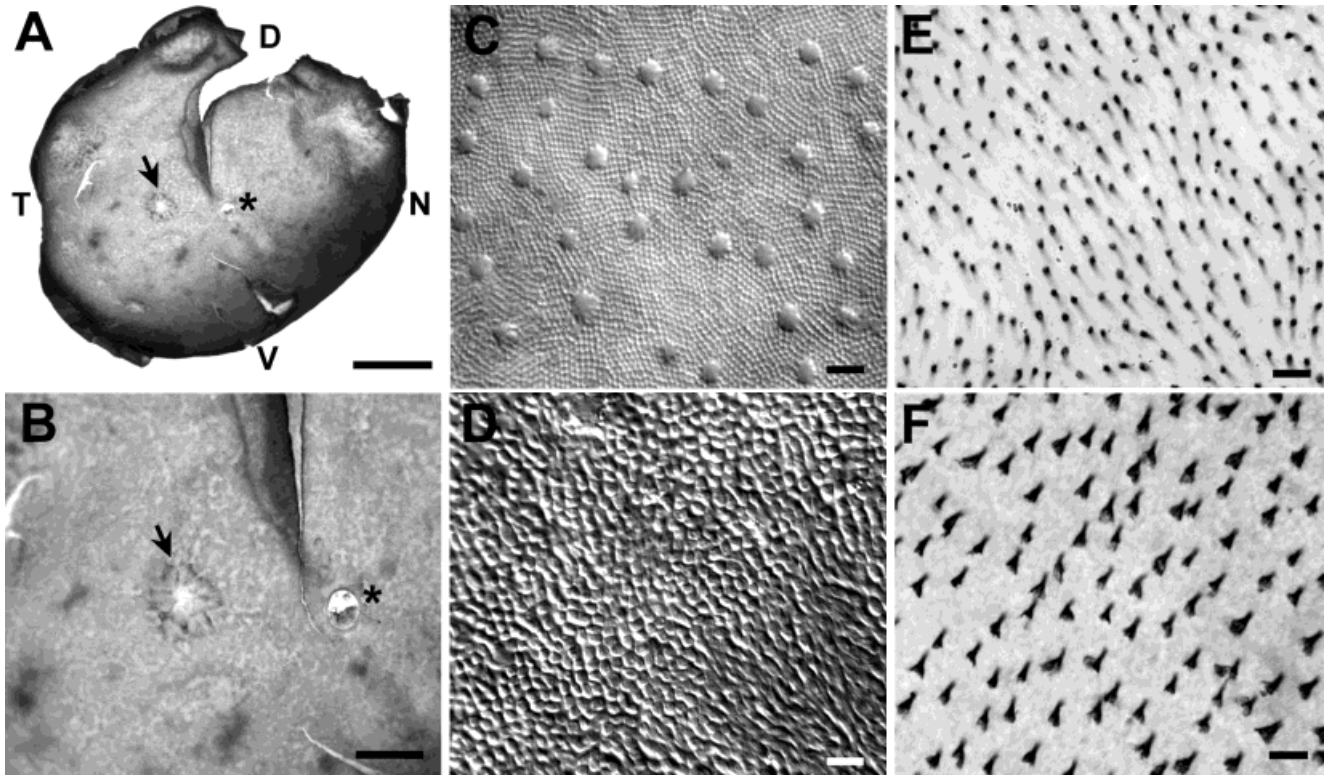


Fig. 1. **A:** Photograph of a freshly removed left retina of the mouse lemur (viewed from the photoreceptor side) showing the optic disk (asterisk) and the area centralis located temporally (arrow). D, dorsal; V, ventral; N, nasal; T, temporal. **B:** The same region shown at higher magnification. **C,D:** Photomicrographs of cones and rods using DIC in a retinal flatmount. Note the larger diameter of cones compared with rods near the area centralis (C) and the increase of the diameter of rods at the retinal periphery (D). In this image, cones are not evident due to the plane of focus. **E** (central retina) and **F** (periphery) illustrate the increase in the diameter of cones labeled with PNA lectin. Scale bars = 2 mm in A, 1 mm in B, 10 μm in C-F.

of a freshly removed unstained retina shows a well-defined avascular area located 2 mm temporal to the optic disk. The outside diameter of this area measured 0.86 mm and corresponds to the area centralis, as defined by the topography of blood vessels and nerve fiber bundles (Figs. 1A,B; Cooper et al., 1979; Stone and Johnston, 1981).

Initial observations in unstained flatmount retinas of the mouse lemur by using DIC optics allow clear discrimination between cone and rod photoreceptors (Figs. 1C-F). Cones have a larger diameter inner segment and constitute a small population of photoreceptor cells whereas rods are thin and more numerous. This was subsequently confirmed by using PNA lectin, which binds to the extracellular matrix of cones, and visualized with DAB as a chromogen in wholemounted and in retinal sections.

MW/LW cones in the mouse lemur

Immunostaining of mouse lemur retinal sections by using the two anti-MW/LW opsin antibodies (the polyclonal CERN956 and the monoclonal COS-1) revealed that almost all cones contain MW/LW opsin. These antibodies, visualized with either DAB or with a fluorescent probe, label selectively and identically the outer segment of MW/LW cones. No immunoreactive label is observed in any rodlike structures. This was confirmed by using double labeling with PNA lectin, which specifically binds to the extracellular matrix of all cones (Figs. 1E,F). All the MW/LW cones immunopositive for CERN956 or COS-1 are also PNA positive (Fig. 2).

The outer segment of MW/LW cones appears extremely long and thin except for a distinct swelling in the mid region. In DAB-stained wholemounts (Fig. 3A), this swelling of the outer segment is illustrated more dramatically than in retinal sections (Fig. 2). This swelling was seen systematically in all cones in the mouse lemur, but we have never observed this feature in other primate or nonprimate species. The total length of the inner and outer segment is 45.55 ± 1.1 μm (n = 20) whereas the length of the entire cone photoreceptor is 89.4 ± 1.8 μm (n = 20). The outer segment is approximately 32.3 ± 0.4 μm (n = 50). The diameter of the inner and outer segment is 2.9 ± 0.08 μm (n = 40) and 2.24 ± 0.04 (n = 20), respectively, whereas the swelling in the mid region of the segment can attain 5.5 ± 0.09 μm (n = 40). These measures were done 2–3 mm temporal from the area centralis and are in the range of that for other primates (Ahnelt and Kolb, 2000). In the retinal periphery, the size of the cones and the swelling increase (Figs. 1E,F). Both opsin antibodies show label only in the proximal region of the outer segment, including dense label in the region of the swelling. In all retinas observed, the extreme distal portion was always devoid of opsin staining. In contrast, PNA labeled the entire extracellular matrix of the outer segment as well as

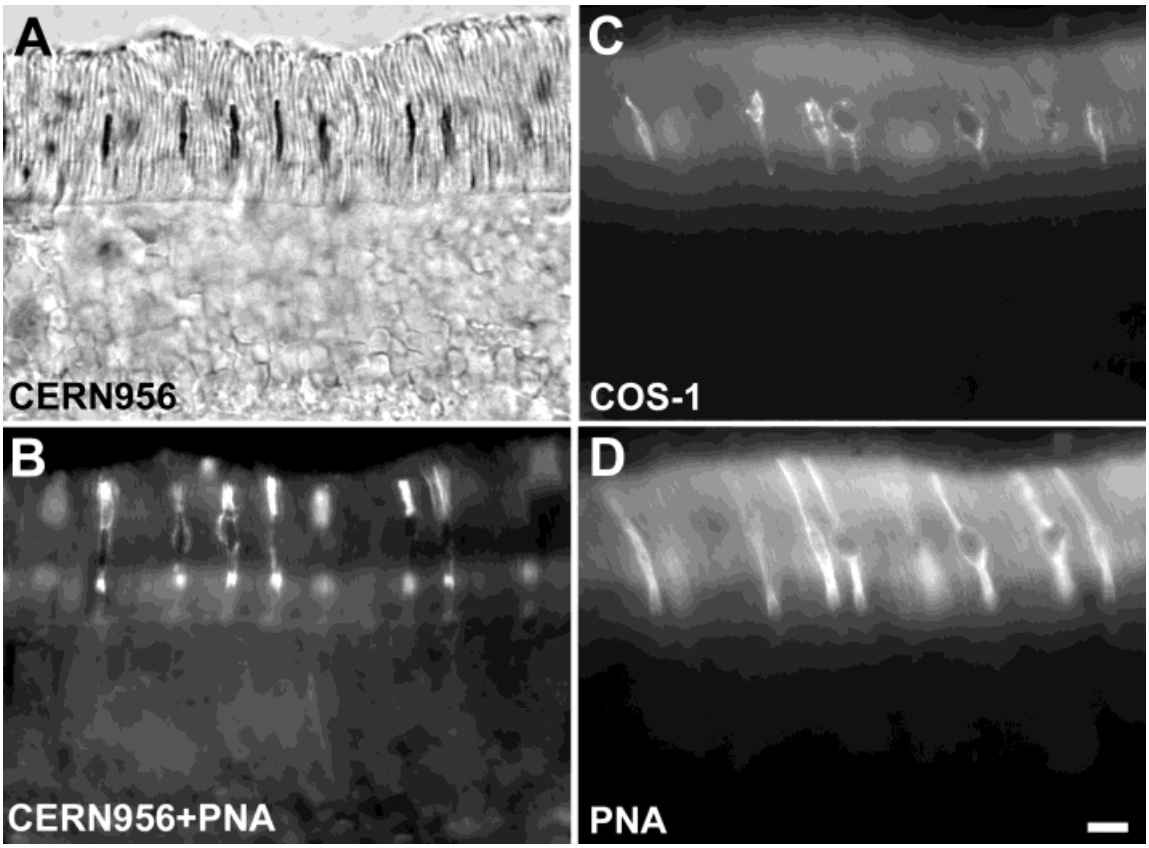


Fig. 2. Photomicrographs comparing MW cone labeling in retinal sections of the mouse lemur using two specific antibodies against MW/LW cones, **(A)** a polyclonal CERN956 (DAB) and **(C)** a monoclonal COS-1 (fluorescence). **B,D:** In both cases, these retinal sections were also labeled with PNA lectin, which binds specifically to the extracellular matrix of all cones. Note that almost all cones are MW. CERN956 and COS-1 label identically the thin outer segment except for a distinct swelling in the mid region using either DAB or a fluorescent probe. Note that all cones CERN956 or COS-1 positive are PNA positive. PNA lectin labels strongly the outer and inner segment of the cone population and very weakly the cell body and the cone pedicle. Scale bar = 10 μm.

the inner segment (Fig. 2), indicating that the cone matrix sheath may well exceed the length of the outer segment. In particular, the region of the connecting cilium is densely labeled. The cell body and pedicle are only lightly visible from the PNA staining.

Depending on retinal location, we noticed that a few cone outer segments not labeled with the MW/LW antibodies are nevertheless PNA positive (Figs. 3C,E). In retinal wholemounts, the frequency of PNA-positive MW/LW opsin-negative cones was extremely low. This result suggested that cones other than the MW/LW cones (possibly SW cones) are present in the retina of *Microcebus*.

SW cones in the mouse lemur

To determine whether SW cones are present in the mouse lemur, we used the SW cone-specific monoclonal OS-2 and the polyclonal JH455 antibodies. All attempts with the OS-2 antibody gave negative results, regardless of the technique of visualization (DAB or fluorescent probe). Increasing the concentration of this antibody severalfold also led to negative results (although in this case, the rod outer segments showed some label; see also Röhlich and Szel, 1993). In contrast, a small number of photoreceptor outer segments are labeled with JH455 antiserum. This antibody is known to bind specifically to SW cone opsins in several primate and nonprimate species.

Considering the contradictory results with the two anti-SW opsin antibodies, we used both simultaneously in combination with the PNA lectin. The JH455 antibody labels rare cones that are PNA positive but OS-2 negative (Figs. 3B,D,F). The morphology of these SW-positive cones appears to be similar to that of the MW cones. The polyclonal SW opsin antibody labels the outer segment (except for the distal extremity) and labels lightly the inner segment and cell body (Figs. 4A,C). The rareness of SW-positive cones in comparison to the entire cone population is shown in a low magnification retinal wholemount labeled with PNA (Fig. 4C).

In order to confirm that the SW opsin antibodies identify SW cones in other primates, combined labeling with a mixture of OS-2 and JH455 was performed in macaque and marmoset retinas. Both antibodies label SW cones in these two species although they have never been used simultaneously. In the macaque and marmoset, OS-2 and JH455 label the same SW cone population whereas in the mouse lemur, only the JH455 antibody labels the SW cones (Fig. 5). Unlike OS-2 immunodetection (Szel et al., 1988), the polyclonal antiserum JH455 labels the entire

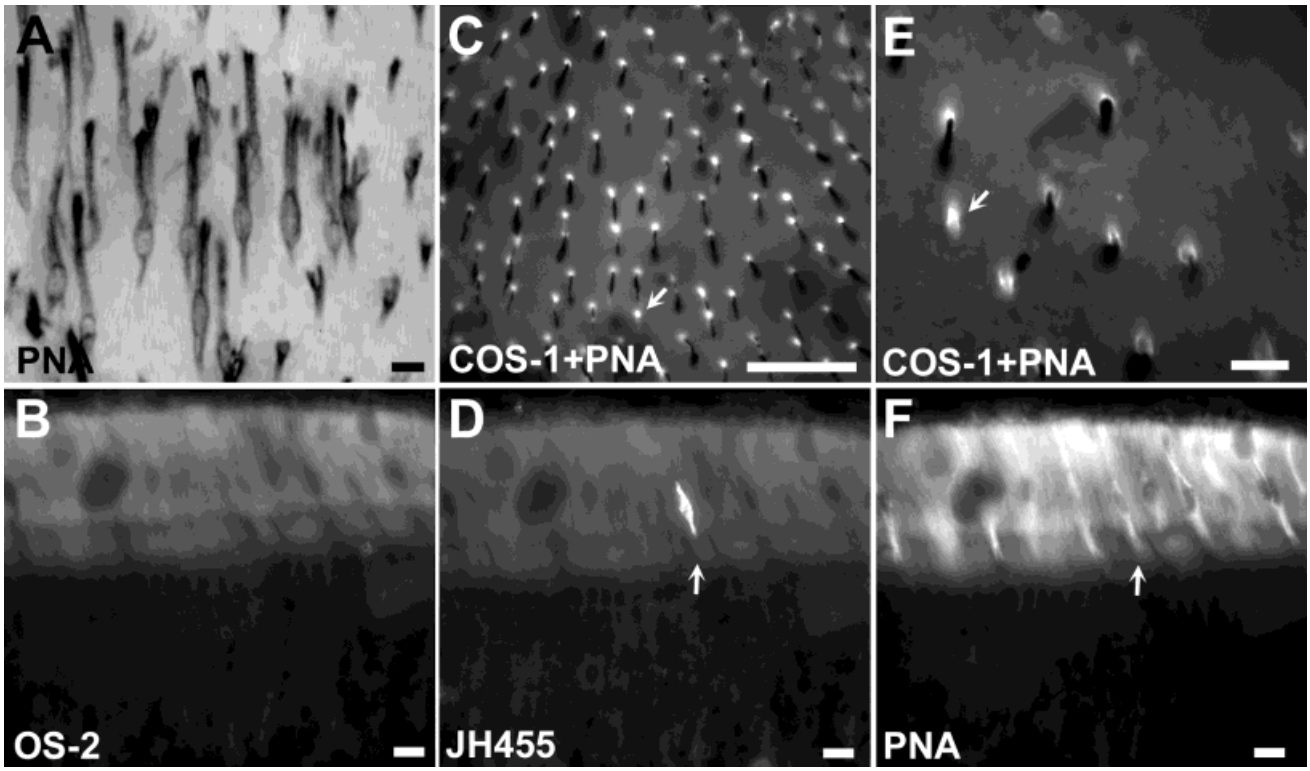


Fig. 3. **A:** PNA-positive cones in a flatmount retina stained with DAB. Note the long and thin outer segments of PNA-positive cones with the distinct swelling in the mid region. **C,E:** In flatmount retinas double labeled by COS-1 and PNA, a minority of cones that are COS-1 negative but PNA positive (white arrow in C and E) are shown at low and high magnification. **B,D,F:** Multiple labeling of cones using OS-2, JH455, and PNA lectin in the same retinal section. Note that the OS-2 antibody shows negative staining whereas a single cone is double labeled by JH455 and PNA, suggesting the presence of a small proportion of SW cones. Scale bars = 10 μm in A,B,D-F, 50 μm in C.

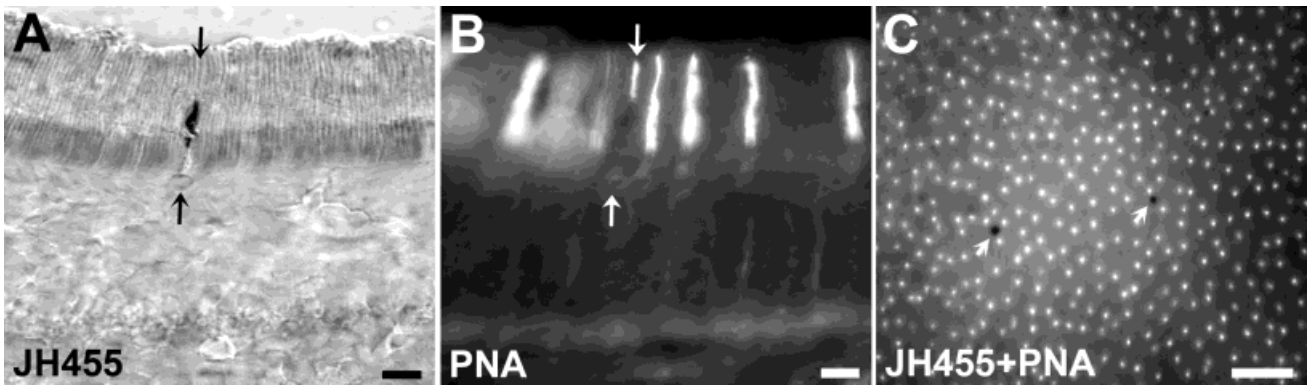


Fig. 4. Double labeling of SW cones using JH455 and PNA lectin in retinal sections **(A,B)** and in a flatmount of the mouse lemur **(C)**. Note that the polyclonal JH455 antibody labels weakly the cell body and strongly the outer segment (A) except for the distal extremity, which is only visualized by PNA (B, in between arrows). (C) The rareness of SW cones in comparison to the entire cone population is shown at low magnification in a flatmount double labeled by JH455 (visualized by DAB, white arrows) and PNA visualized by immunofluorescence. Scale bars = 10 μm in A,B, 50 μm in C.

SW cone in the macaque and marmoset (densely the outer segment and more lightly the inner segment and the cone pedicle).

In order to confirm that the SW cones do not represent a subpopulation of MW cones (cones with both opsins or a cross-reaction of the SW cone antibody in some MW cones), we did a multiple labeling by using a mixture of JH455 and COS-1 antibodies, followed by labeling with PNA lectin. The localization of SW and MW cone antibodies shows a complementary pattern of staining in the PNA-positive cones (Fig. 6). In no case, cones stained by COS-1 were labeled by JH455 and vice versa. It is obvious that the SW cones constitute a minority of the cone population in the mouse lemur.

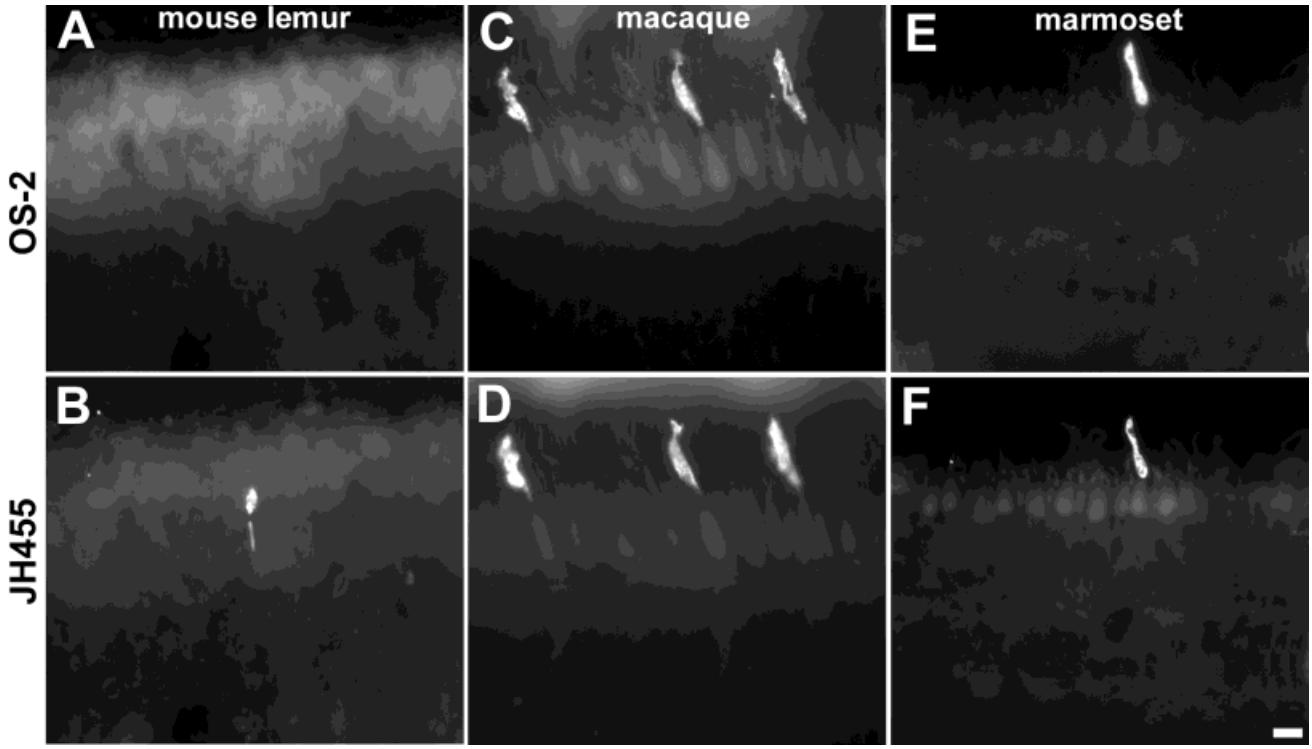


Fig. 5. Comparison of immunofluorescent double labeling of SW cones using OS-2 and JH455 in the same retinal section of the mouse lemur **(A,B)**, macaque **(C,D)**, and marmoset **(E,F)**. In the macaque and marmoset, these two antibodies label the same SW cone population. In the mouse lemur, SW cones are only visualized with the JH455 antibody. Scale bar = 10 μm.

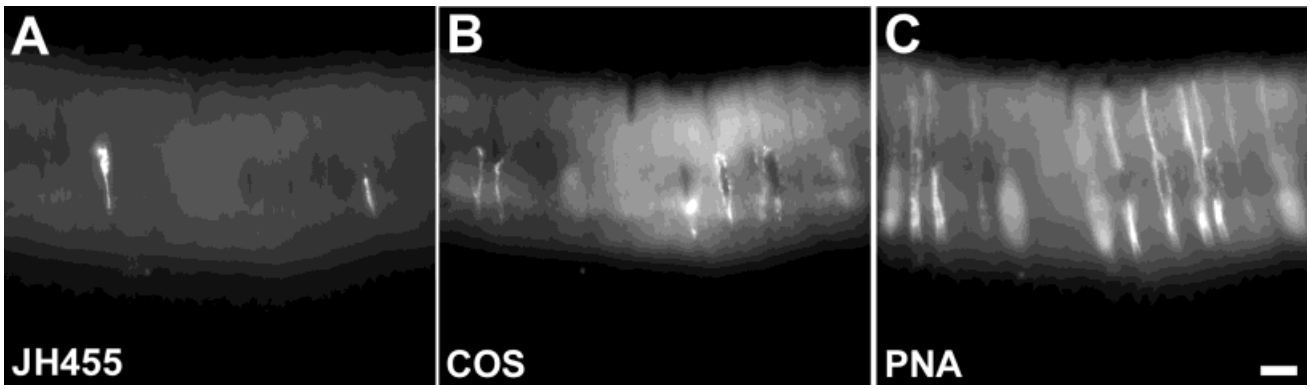


Fig. 6. Immunofluorescent multiple labeling of SW **(A)** and MW **(B)** cones using JH455 and COS-1 antibodies in the same retinal section of the mouse lemur. Cones stained by JH455 were not labeled by COS-1, demonstrating that SW cones do not represent a subpopulation of MW cones. PNA staining shows the complementary pattern of label of both SW and MW cones **(C)**. Scale bar = 10 μm.

Spatial distribution of cones

The spatial distribution of all cones identified by PNA lectin staining was determined from counts on retinal wholemounts by using a computerized plotting system. Cones show a centroperipheral gradient with the highest density located in the temporal region of the retina (Figs. 7A,B). Peak densities were about 7,500–8,000 cones/mm^2. The minimum density in the periphery was approximately 1,000 cones/mm^2, corresponding to a centroperipheral gradient of about 1 to 7–8. The general distribution shows a broad horizontal component through the mid nasotemporal region of the retina with cone densities above 4–5,000 cones/mm^2. The cone density decreases less sharply in the inferior half compared with the superior half of the retina. Immunoreactive cones form a regular mosaic in different areas of the retina (Figs. 1E,F, 4C).

Distribution of MW cones

The distribution of MW cones resembles closely the distribution of all cones as seen from the PNA staining

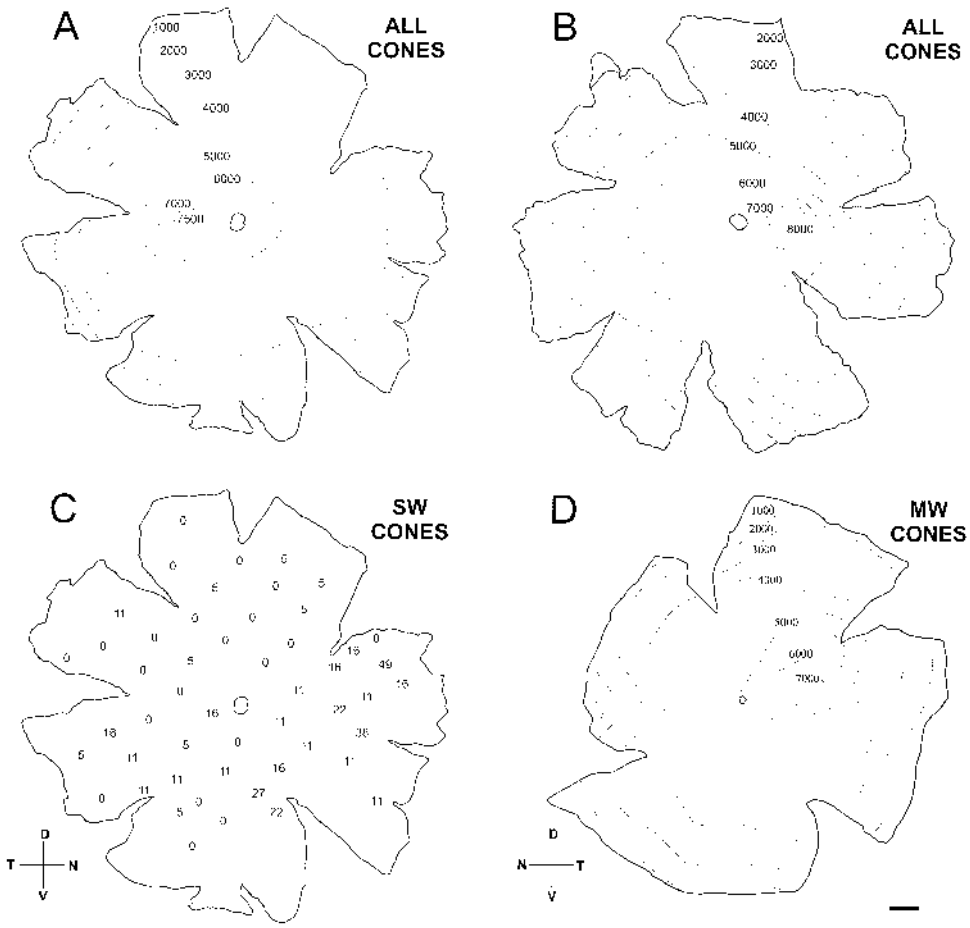


Fig. 7. Isodensity maps of the distribution of all cones **(A,B)**, SW cones **(C)**, and MW cones **(D)** in retinal wholemounts of the mouse lemur. Values indicate the density of photoreceptors per mm^2 for a given isodensity contour. The white circle corresponds to the optic disk. The spatial distribution of all cones identified by the PNA staining shows a centroperipheral gradient with a peak in the temporal region (7,500–8,000 cones/mm^2) and a decrease to 1,000 cones/mm^2 at the retinal periphery (A,B, retinas from two individuals). MW cones show a similar distribution with a peak localized at the area centralis (D). The distribution of SW cones as determined by using the JH455 antibody (C). Isodensity contours are not calculated due to the irregular and low densities. This is the same retina double labeled with the PNA lectin shown in A. Note the irregular distribution of SW cones over the retinal surface with higher numbers in the nasal region. D, dorsal; V, ventral; N, nasal; T, temporal. Scale bar = 1 mm.

(Fig. 7D). The peak density in the area centralis is slightly lower, approximately 7,000 cells/mm^2. This is not unexpected because PNA labels both the inner and outer segments, whereas the MW/LW antibody only labels outer segments which are more fragile and thus more susceptible to be lost during processing. Densities were generally higher in the inferior part of the retina and decreased at the periphery to 1,000 cells/mm^2.

Distribution of SW cones

SW cones are located mainly in the nasal part of the retina and the densities are extremely low with a peak density reaching only 49 cones/mm^2 (Fig. 7C), whereas the temporal region contains few or no SW cones. The highest density measured was 49 cells/mm^2 in a single count although densities were mainly between 0–11 cells/mm^2. SW cones are present in low but consistent densities around the entire periphery of the retina, except in the temporal region. Their distribution is irregular because areas that contain cones are adjacent to areas that are devoid of SW cones. For example, at low magnification, empty zones are seen in between areas with sparsely distributed SW cones (Fig. 8A). In certain areas, SW cones are arranged linearly or they are clustered. Figures 8B and 8C show zones with a few SW cones adjacent to a zone with a higher concentration of almost regularly arranged SW cones.

Spatial distribution of rods

The spatial distribution of rods was determined from counts on retinal wholemounts by using DIC optics. Rods show a centroperipheral gradient with the highest density located in the temporal part of the retina (Fig. 9). Peak densities were 700,000–850,000 cells/mm^2. The minimum density in the periphery was approximately 100,000 rods/mm^2. Thus, the central to peripheral gradient in rod density was about 7–8.5-fold, which was similar to that of cones. The peak in rod density coincides with the area of peak cone density and the area centralis. The difference in the size of rods between the center and the periphery is

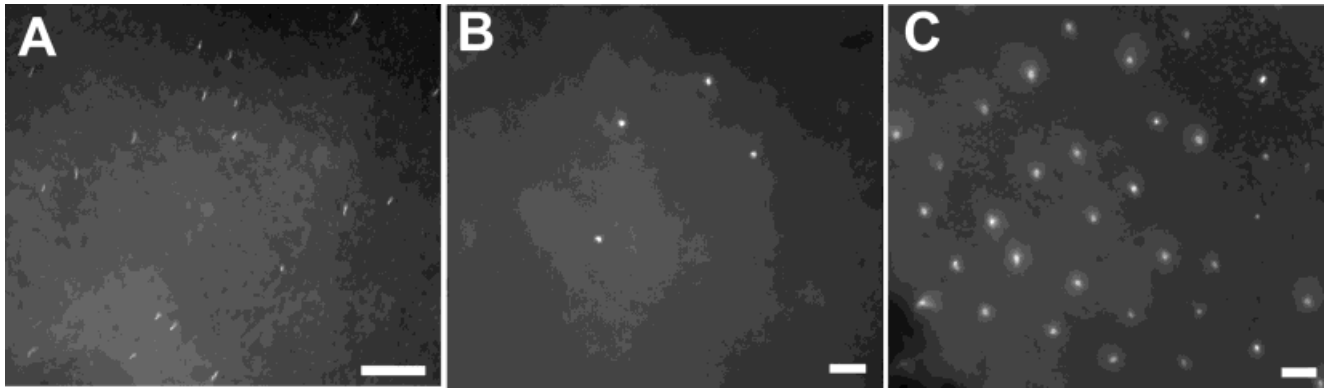


Fig. 8. Immunofluorescent labeling of SW cones (JH455 antiserum) in a flatmount retina of the mouse lemur illustrating the irregular distribution of SW cones at low **(A)** and high magnifications **(B,C)**. B and C show adjacent areas containing a sparse (B) and higher (C) concentration of SW cones. Scale bars = 100 μm in A, 10 μm in B,C.

quite evident by using DIC optics (Figs. 1C,D). Rods are thinner and are found in high numbers in the center of the retina whereas their number decreases at the periphery and their diameter increases.

Total numbers of rod and cone photoreceptors

The mean surface area was measured from seven fixed but undehydrated retinal wholemounts of the mouse lemur. The surface area ranges from 128 to 137 mm^2 with an average of 132 mm^2. Based on this mean retinal area, the total number and ratio of different photoreceptors was determined. The total number of rods is 65,800,000 (ranging from 64,950,000 to 67,390,000 rods per retina, n = 3) and the total number of cones is 576,000 (ranging from 530,000 to 610,000 cones per retina, n = 5), giving a ratio of 1 cone to 114 rods. The total number of MW cones counted is 506,400 (ranging from 486,000 to 525,000 MW cones per retina, n = 2) and the total number of SW cones is 1,141 (n = 1). Therefore, the ratio is 1 SW cone to 444 MW cones, 1 MW cone to 130 rods, and 1 SW cone to 57,700 rods.

Spatial distribution of rods and cones in relation to ganglion cell layer neurons

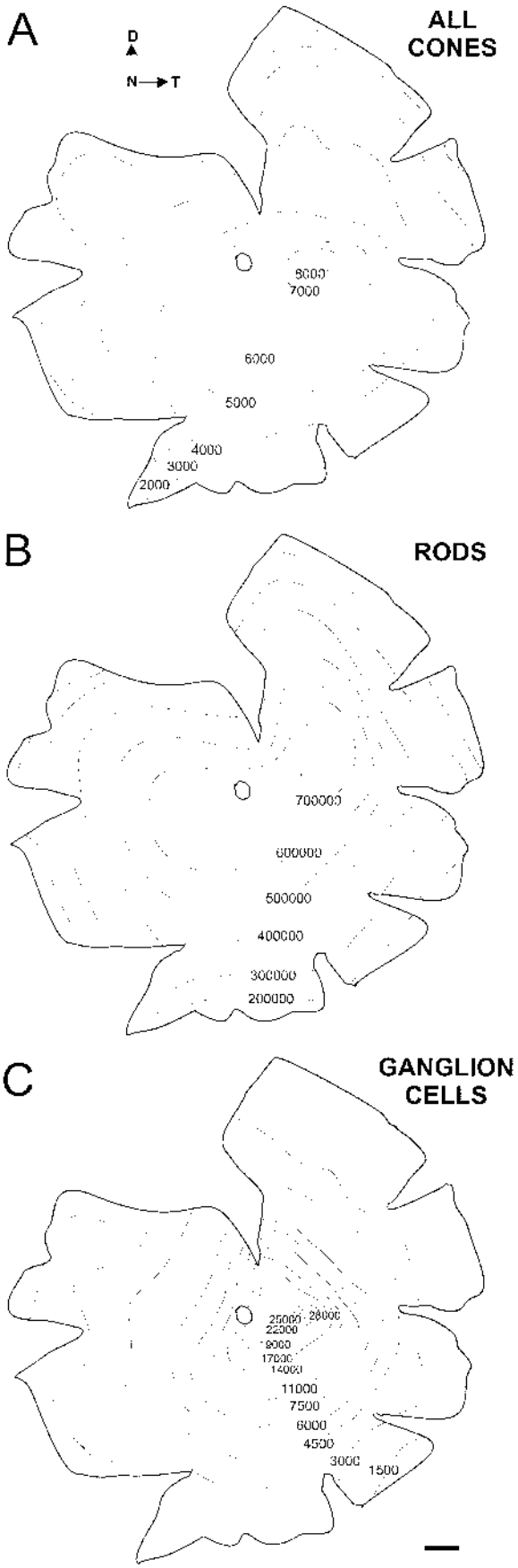
Figure 9 represents an isodensity map of cones, rods, and cell density in the ganglion cell layer as determined in the same retina. Cones were visualized by using PNA lectin labeling, rods by using DIC optics, and ganglion cell layer neurons with cresyl violet cytochemistry. Cone and rod distribution was described in the previous paragraph. The distribution of ganglion cell layer neurons was estimated by using the computerized plotting system from counts of all cells in the ganglion cell layer. This latter count includes ganglion as well as displaced amacrine cells and is probably an overestimate of the actual number of ganglion cells.

Ganglion cell layer neurons show a centroperipheral gradient, with the highest density located in the temporal region of the retina. Peak density in the area centralis is 28,000 cells/mm^2. The minimum density in the periphery was approximately 1,500 cells/mm^2, corresponding to a sharp centroperipheral gradient of about 18 to 1. The density of ganglion cell layer neurons increases gradually from 1,500 cells/mm^2 in the periphery to 6,000 cells/mm^2 in the mid region of the retina. This increase becomes steeper from the mid part of the retina (near the optic disk) toward the area centralis (approximately fivefold) where neurons in the ganglion cell layer are highly concentrated. In this retina, it was possible to align precisely the morphological thickening of the area centralis and the peak density of cones, rods, and neurons in the ganglion cell layer.

Figure 10 represents the densities of rods, cones, and ganglion cell layer neurons calculated from the same retina at different distances from the area centralis along the horizontal and vertical axes. The region of peak photoreceptor and ganglion cell layer neuron density coincides at the area centralis. Densities of photoreceptor (cones and rods) and neurons in the ganglion cell layer are higher in the nasal part of the retina compared with the temporal region. For example, density decreases more slowly from the area centralis toward the nasal periphery. If the densities of photoreceptors and neurons in the ganglion cell layer are normalized (Fig. 10B), the proportional changes in the number of cones match closely those of the ganglion cell layer neurons at 2 mm around the area centralis. From this distance to the periphery, the density of neurons in the ganglion cell layer decreases more rapidly than that of rods and cones, suggesting an increase in the convergence of photoreceptors on ganglion cells toward the periphery.

Photoreceptor ratios

Rod-to-cone ratio. The rod-to-cone ratio is relatively constant (approximatively 100 rods for 1 cone) around the area centralis to an eccentricity of 2–3 mm toward the nasal or temporal axes (Fig. 11). This ratio then increases toward the nasal part of the retina to attain 140 rods for one cone, which may be linked to the more gradual decrease of rod densities in this region compared with cone densities (Figs. 10, 11). In contrast, this ratio remains relatively constant from the area centralis to the periphery of the retina in the temporal region. The ratio of rods to cones along the vertical axis increases from the area centralis to the dorsal part of the retina but declines



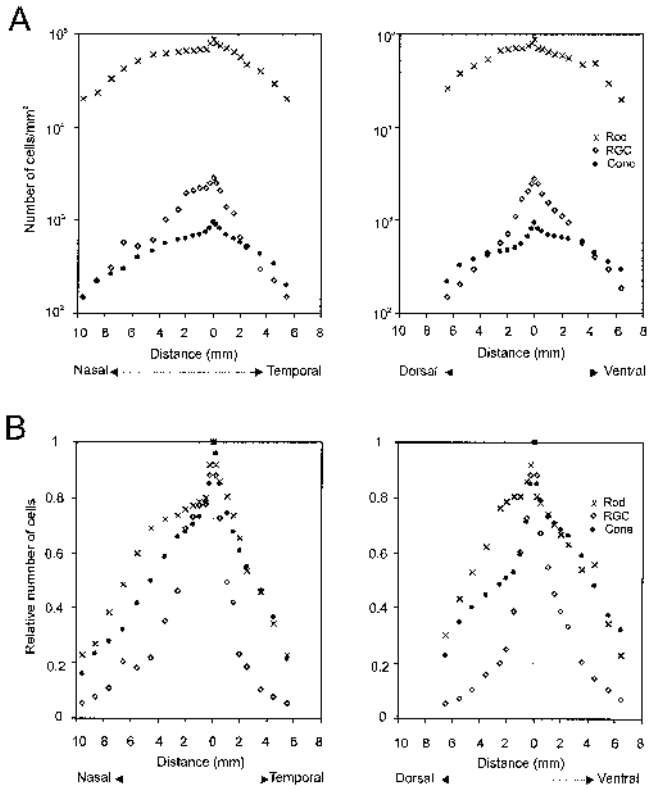


Fig. 10. **A:** Graphs representing the densities of rods, cones, and ganglion cells calculated from the same retina (presented in Fig. 9) at different distances along the horizontal and vertical axes through the area centralis. Note that the peak densities of both classes of photoreceptors coincide with those of the ganglion cells in the area centralis. **B:** Normalized distribution of the density of photoreceptors and ganglion cells along the two axes. The proportional changes in the number of cones match closely those of the ganglion cells at 2 mm around the area centralis. From this distance to the periphery, ganglion cell density decreases more rapidly than that of the rods and cones. The gray line represents the region of the area centralis.

toward the ventral part of the retina. The ratio of rods to cones is relatively stable in the temporal and ventral regions of the retina because the decrease of the density of cones parallels that of rods.

Ratio of rods and cones in relation to ganglion cell layer neurons. Figure 11 shows a similar change in the ratios of cones or rods in relation to neurons in the ganglion cell layer. The ratio of cones to neurons in the ganglion cell layer is relatively constant across the retina. In the area centralis, there is one cone for three neurons in the ganglion cell layer, whereas the ratio is one neuron in the ganglion cell layer for 1.5 cones in the periphery. Note

Fig. 9. Isodensity maps of cones **(A)**, rods **(B)**, and ganglion cells **(C)** determined from the same retinal wholemount of the mouse lemur. The distribution of cones is similar to that shown in Figures 7A,B. Rod distribution shows a centroperipheral gradient with the peak including and extending slightly dorsal to the area centralis. The distribution of ganglion cells shows the same centroperipheral gradient with the peak located at the area centralis. The area centralis of this retina is shown in Figure1A,B. Scale bar = 1 mm.

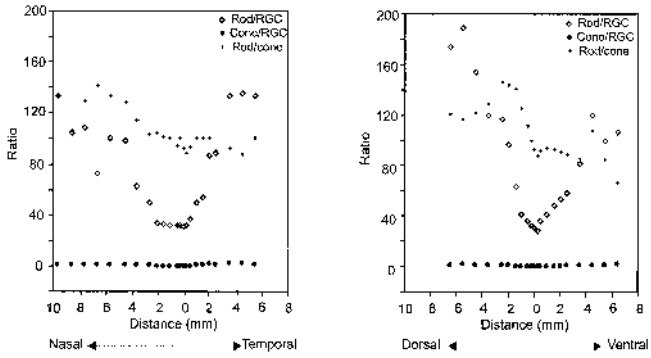


Fig. 11. Representation of the ratio of rods to ganglion cells, cones to ganglion cells, and rods to cones along the horizontal and vertical axes of the retina. The rod-to-cone ratio is relatively constant (approximatively 100 rods for one cone) around the area centralis to an eccentricity of 2–3 mm toward the nasal or temporal region. This ratio then increases toward the nasal part of the retina to attain 140 rods for one cone. Note that along the vertical axis, the ratio of rods to cones increases from the area centralis to the dorsal part of the retina but declines toward the ventral part. The ratio of cones to ganglion cells is relatively constant across the retina. In the area centralis, there is one cone for three ganglion cells. In the periphery, the ratio is one ganglion cell for 1.5 cones. Rods show a sharper gradient in relation to ganglion cells. In the area centralis, the ratio is about 30 rods per ganglion cell and remains constant along the nasal axis for 2–3 mm. This ratio increases to 140 rods per ganglion cell toward the nasal and temporal periphery of the retina. In the dorsal margin, the ratio is 180:1. The gray line represents the region of the area centralis.

that these counts in the ganglion cell layer do not distinguish "displaced" between distinguish and amacrine from ganglion cells. Therefore, the actual ratios may be slightly lower. This shows a fairly low and regular degree of convergence between cones and neurons in the ganglion cell layer across the retina. Rods show a sharper gradient in relation to ganglion cell layer neurons. In the area centralis, the ratio is about 30 rods per neurons in the ganglion cell layer. This ratio remains constant along the nasal axis for 2–3 mm, in relation to the horizontal component of the distribution gradients. Toward the nasal and temporal periphery of the retina, the ratio increases to 140 rods per neurons in the ganglion cell layer, whereas the ratio is 180:1 in the dorsal margin.

Spatial resolution

By using the measures for eye size and cell counts in the area centralis in *Microcebus*, we calculated the theoretical spatial resolution of the retinal system (Peichl and Wassle, 1979; Pettigrew et al., 1988; Yamada et al., 2001).With an eye size (anteroposterior distance) of 9.65 mm, the posterior nodal distance (PND) equals 5.00 mm. This corresponds to a linear retinal magnification factor of 0.087 mm per degree. A retinal ganglion cell density in the area centralis of 28,000 cells/mm^2 would allow a maximum spatial resolution of 7.8 cycles per degree. However, as mentioned above, this is probably an overestimation because our counts do not distinguish displaced amacrine cells from ganglion cells in the ganglion cell layer (see also discussion below on P ON and OFF cells). The cone density in the area centralis is relatively lower and the sampling characteristics of this array yield a spatial resolution of only 4.2 cycles per degree. The potential rod input is much higher in the area centralis and the spatial resolution calculated from the rod density is >40 cycles per degree. This is correlated with a higher degree of convergence of rods onto neurons in the ganglion cell layer (30:1 ratio).

DISCUSSION

Presence of SW cones in the mouse lemur

Although SW cone photoreceptors are a characteristic feature of diurnal primates, anatomical, behavioral, and electrophysiological studies show that two nocturnal primates, the owl monkey (*A. trivirgatus*) and the bushbaby (*Otolemur crassicaudatus*), lack functional SW cones (Wikler and Rakic, 1990; Jacobs et al., 1993, 1996b). These two species appear to have SW cone gene defects with deleterious mutational changes that introduce a premature stop codon (Jacobs et al., 1996b). The nocturnal Strepsirrhine, *Loris*, may also lack SW cones (Ahnelt and Kolb, 2000). A major outcome of our study is the identification of a small population of SW cones in the nocturnal mouse lemur by using specific antibodies against the different cone opsins. Surprisingly, SW cones are only recognized in this species by the JH455 antiserum whereas the monoclonal OS-2 antibody fails to detect any photoreceptors. This is the first observation of a complete difference in the labeling pattern between these two antibodies, although Bumsted et al. (1997) described in the macaque that OS-2 is more sensitive than JH455 in detecting low levels of SW opsin protein. The anti-SW opsin JH455 labeling is specific to SW cones in the mouse lemur as confirmed by our results. We demonstrate (1) immunopositive labeling of the same cone with PNA lectin and JH455 antibody; (2) complementary staining of cones by using JH455 and COS-1 antibodies, suggesting that the SW cones do not represent a subpopulation of MW cones or that both SW and MW pigments are not colocalized in the same photoreceptor; and (3) in the macaque and marmoset, the SW cone population is labeled by both OS-2 and JH455 antibodies, whereas only JH455 labels this population in the mouse lemur. Previous studies using these two antibodies in a range of species have resulted in identical patterns of label, either similar positive labeling of all the SW cones in horses (Sandmann et al., 1996) or failure to label any cones in seals, African giant rats (Peichl and Moutairou, 1998), and cetaceans (for a recent review, see Ahnelt and Kolb, 2000; Peichl et al., 2001).

The absence of labeling with the OS-2 antibody in the mouse lemur is remarkable because this antibody has been shown to be C-terminal specific and this sequence is relatively highly conserved in visual pigments (Röhlich and Szel, 1993). Although JH455 and OS-2 are reliable detectors of mammalian SW cone opsins (Szel et al., 1988, 1996), they recognize different epitopes in the SW cone opsin: JH455 was raised against a peptide representing the 42 C-terminal residues of the human SW cone opsin (Wang et a.l, 1992), whereas OS-2 was produced against extracts of chicken photoreceptor membranes (Szel et al., 1988). JH455 is a polyclonal antibody and will therefore have a broader epitope repertoire than the monoclonal antibody OS-2. One explanation for the inability of OS-2 to detect SW cones in the mouse lemur could be that the epitope it recognizes in the SW cone opsin is not conserved across primate evolution. Indeed, mouse lemur cones lack some of the markers considered typical of primate cones.

For example, calbindin is not detected in cones in the mouse lemur (Chiquet et al., 1999) and the tarsier (Hendrickson et al., 2000), whereas marmoset, macaque, and human cones all show strong immunoreactivity for calbindin (Chiquet et al., 1999). Possible substitutions in the SW opsin residues in the mouse lemur representing the epitope for OS-2 may have reduced the affinity of the antibody to such an extent that immunolabeling is not detected. Such a fate is much less likely to occur for JH455 because of its much broader epitope repertoire. Furthermore, negative findings in other species concerning SW cones should be interpreted with caution because their presence may be overlooked due to their sparse and irregular distribution.

Number and distribution of SW cones

SW cones are present in the mouse lemur, but in extremely low numbers, representing only about 0.2% of the total cone population. In other primates, SW cones constitute a minority of the entire cone population: 2–10% in the marmoset, macaque, human, and the tarsier (Curcio et al., 1991; Martin and Grünert, 1999; Hendrickson et al., 2000). This proportion also holds in other mammals including the diurnal tree shrew, squirrels, and many nocturnal rodents (Muller and Peichl, 1989; Szel et al., 2000).

A striking characteristic of the SW cones in the mouse lemur is the unusual spatial distribution. SW cones are highly irregularly dispersed with widely variable intercell distances. The main distribution is found in the nasal part of the retina, predominantly in the periphery, whereas SW cones are totally absent from the area centralis and the dorsotemporal quadrant. Density is generally very low, in the range of 0–11 cells/mm^2, with a maximum of 49 cells/mm^2 seen in a single location. Although only one retina was mapped fully, observations on SW cones in several other wholemounts were similar but with interindividual variations in local distribution. A peripheral distribution of SW cones is also observed in the nocturnal tarsier where SW cones represent 9–14% of all cones (Hendrickson et al., 2000). In this species, the density of SW cones is very low in the central retina (less than 1% of all cones), increases symmetrically with eccentricity, and peaks at the periphery.

In Old World monkeys and humans, SW cones form a regular mosaic (Wikler and Rakic, 1990; Curcio et al., 1991; Martin and Grünert, 1999). In several other diurnal primates, SW cones are irregularly spaced (e.g., marmoset, *Ateles*, and some Cercopithecidae; Mollon and Bowmaker, 1992; Martin and Grünert, 1999). Most other mammals (for review, see Szel et al., 1996), including marsupials (opossum), rabbits, cats, horses, rats, and guinea pigs (Szel et al., 1988, 1992; Szel and Röhlich, 1992; Ahnelt et al., 1995; Sandmann et al., 1996), also show an irregularly spaced mosaic or a nonhomogenous spatial distribution across the retinal surface. The horse has been described as having a patchy distribution of SW cones (Sandmann et al., 1996). Thus, a regular mosaic of SW cones is only present in certain primates and in the cone-dominated retina of the tree shrew (Muller and Peichl, 1989).

Number and distribution of MW cones: relation to SW cone distribution

Both nocturnal (bushbaby, *O. crassicaudatus*) and diurnal (*L. catta* and *E. fulvus*) Strepsirrhines have been shown to have a single class of MW/LW cone pigment with a spectral sensitivity of 545 nm. The diurnal lemurs have a SW cone pigment with a peak of about 437 nm (Jacobs and Deegan, 1993). To identify MW/LW cone opsin in the mouse lemur, we used the monoclonal COS-1 and the CERN956 antiserum. CERN956 was raised against a peptide fragment derived from the human red/green-sensitive cones (Vissers and DeGrip, 1996). COS-1 has been shown to be specific to an LW-sensitive, 33 kD cone visual pigment in the chicken (Szel et al., 1986). This antibody recognizes an epitope that is common or very similar in medium to LW pigments in many vertebrate species, from reptiles to humans (Szel et al., 1986, 1988; Cserhati et al., 1989). In the mouse lemur, an MW/LW cone population is detected by using both antibodies.

Quantitative studies in nocturnal primates show that peak density of MW cones is between 7,500 and 8,500 cells/mm^2 in the bushbaby (Wikler and Rakic, 1990) and the mouse lemur (present study). The owl monkey was described originally to have a peak density of 9,000 cones/mm^2, although a more recent study reports the cone density to be 16,300 cells/mm^2 (Yamada et al., 2001). In comparison, peak MW cone density in the tarsier attains 14,200 cells/mm^2 (Hendrickson et al., 2000). The centroperipheral gradient in the mouse lemur and the bushbaby is in the range of 1:7–8, but is lower in the tarsier and the owl monkey (1:4–5). Wikler and Rakic (1990) considered that in the bushbaby and owl monkey, the peak cone density is located 1–2 mm dorsal to the area centralis, whereas Yamada et al. (2001) described the peak cone density in the fovea of the owl monkey. In the mouse lemur, peak density of MW cones is located at the area centralis.

In the mouse lemur, the topographies of SW and MW cones differ markedly from each other. MW cones are distributed concentrically around the area centralis with evidence of a weak horizontal component. The MW cone distribution shows an asymmetry between the dorsal and the ventral retina, with highest densities in the ventral region similar to the description in the tarsier (Hendrickson et al., 2000). Comparison of the SW and MW cone mosaics in the mouse lemur suggests independent developmental mechanisms, indicating that the SW mosaic does not interact with the MW cone mosaic during ontogeny to generate the adult pattern of cone spacing. In fact, the high irregularity of SW cone spacing and regional distribution could reflect defects in the regional regulation of gene expression and protein synthesis in the mouse lemur during development.

Distribution gradients of photoreceptor and ganglion cell layer neurons: the area centralis, spatial resolution, and sensitivity

The transition from the area centralis to the fovea is believed to have evolved in early primates in relation to the predominance of central vision, acuity, and the change from nocturnal to diurnal behavior (Ahnelt and Kolb, 2000; Kay and Kirk, 2000). In diurnal primates, cones occupy the center of the fovea, whereas the region of peak rod density is reported to be located 2–4 mm dorsal to the foveal area (Packer et al., 1989). Wikler and Rakic (1990) also reported that in nocturnal primates (owl monkey and bushbaby), peak rod density is located dorsal to the area centralis. However, a recent study by Yamada et al. (2001)

TABLE 1. Eye Size, Retinal Magnification Factors, and Spatial Resolution in Nocturnal Primates[1]

Species	Eye size (or PND) in mm	Retinal magnification factor (mm/degree)	Peak density (cells/mm^2)	Theoretical spatial resolution (cycles/degree)	Measured spatial resolution (cycles/degree)
Microcebus	9.65 (PND = 5.00)	0.087	RGC 11,000	4.9	
			Cones 8,000	4.2	
			Rods 900,000	43.2	
Galago	18.26 (PND = 9.65)(1)	0.165	RGC 4,800(3)	6.2	Behavioral studies: 4.8–6(5); 3.5–7.5(6); 5–6.6(7)
			Cones 8,500(4)	8.2	Electrophysiological studies: 5–7(8)
			Rods 450,000(4)	59.7	
Aotus		0.20(2)	RGC 6,000(2)	8.3(2)	Electrophysiological study: 10(9)
			Cones 16,300(2)	13.7(2)	
			Rods 388,000(2)	66.9	

[1]Spatial resolution calculated from the ganglion cell population in *Galago* and *Aotus* is slightly higher (six to nine cycles per degree) than in the *Microcebus* (see Discussion for details of ganglion cell numbers). This is not unexpected due to the higher retinal magnification associated with the larger eye size. The theoretical resolution of the rod and cone systems in these other species is also higher, but only by a few cycles per degree. Behavioral and electrophysiological studies of spatial resolution and contrast sensitivity are in agreement with the theroretical values calculated from the retinal parameters. References: (1) Dodt, 1967; (2) Yamada et al., 2001; (3) DeBruyn et al., 1980; (4) Wikler and Rakic, 1990; (5) Langston et al., 1986; (6) Ordy and Samorajski, 1968; (7) Treff, 1967; (8) Bonds et al., 1987; (9) Jacobs, 1977.

in the owl monkey showed that both rod and cone densities peak in the area centralis. We also found that rod density peaks at the area centralis in the mouse. This region of high rod density at the area centralis may be an important feature of the visual system in nocturnal primates, allowing a specialization for high scotopic sensitivity. This issue of a central area of rod specialization in nocturnal compared with diurnal primates has also been discussed by Yamada et al. (1998, 2001).

In *Microcebus*, the distribution of both rods and cones is characterized by a centroperipheral gradient. This gradient is quite similar for the population of both cones and rods (1:8 and 1:9, respectively). The region of maximum density of cones, rods, and ganglion cell layer neurons coincides at the area centralis. However, the gradient of the ganglion cell layer neurons (1:18) is twice that of the photoreceptor populations, reflecting the predominance of central vision in relation to both photoreceptor types and an increased degree of convergence of photoreceptors on ganglion cells toward the periphery. This is particularly evident for rods where the ratio varies from 30:1 in the center to almost 180:1 in the periphery. Ratios of cone to ganglion cell layer neurons increase only slightly toward the periphery—from one cone for three ganglion cell layer neurons in the area centralis compared with 1.5 cones per ganglion cell layer neuron at the periphery. This is much less than the increase in convergence reported for diurnal primates or the nocturnal busbaby and owl monkey, which varies from one to three cones per ganglion cell layer neurons in the fovea to >60 cones per ganglion cell layer neurons at the periphery (Goodchild et al., 1996; Yamada et al., 1998, 2001).

The relationships among cell gradients, retinal magnification, and spatial resolution at the area centralis can be understood better when considered together in relation to the nocturnal habits of the mouse lemur. The spatial resolution afforded by the density of the ganglion cell layer neurons in the area centralis is 7.8 cycles per degree. This value for maximum resolution should be interpreted with caution. First, our counts include all neurons in the ganglion cell layer, including displaced amacrines, which can account for a significant proportion of the total number of cells. Second, ganglion cells in primates comprise two distinct pathways, the P and M pathways projecting, respectively, to the parvocellular and magnocellular layers of the lateral geniculate nucleus. The P pathway is characteristic of higher spatial resolution and chromatic vision, whereas the M pathway has lower spatial resolution and conveys luminance information (Kremers and Weiss, 1997; Lee et al., 1997). The P ganglion cells with smaller dendritic fields typically set the limit on spatial resolution (Yamada et al., 1998, 2001). However, the proportion of P and M ganglion cells in the mouse lemur is currently unknown. Nevertheless, if P cells account for 80% of the population as in other primates (Perry et al., 1984), the peak of P cells would correspond to about 22,400 cells/mm^2. These P cells occur as ON and OFF cells in a 50:50 ratio. The ON and OFF populations act as independent separate sampling arrays (Wässle and Boycott, 1991; Yamada et al., 2001), hence the density relevant for the calculation of spatial resolution is about 11,000 cells/mm^2. By using this density, the theoretical spatial resolution of mouse lemur ganglion cells is 4.9 cycles per degree. This is close to the calculated cone resolution of 4.2 cycles per degree in the area centralis. This represents a reasonable photopic spatial resolution for a nocturnal animal that is occasionally active at higher light levels at dawn and dusk (Pariente, 1980). Maximum spatial resolution calculated from rod density is much higher (>40 cycles per degree) and the convergence of many rods onto ganglion cell layer neurons (30:1 ratio) allows a high level of luminous sensitivity. This spatial resolution is limited obviously by that of the ganglion cell array. Yamada et al. (2001) also reported that the high rod convergence in nocturnal primates allows better sensitivity at low light levels, in contrast to diurnal primates in which rod convergence in the central retina is much lower.

This spatial resolution is slightly lower than that of other nocturnal primates for which data are available (*Galago*, *Aotus*), as calculated from the magnification factor, ganglion cell and photoreceptor densities, and from behavioral and electrophysiological data (see references in Table 1). The species with larger eye size and, consequently, higher retinal magnification show increased values of spatial resolution.

Adaptation of the retina to the nocturnal habitat also involves several mechanisms that increase luminous sensitivity. This is an important consideration because light levels in the Malagasy forest at night when animals are actively leaping are in the range of 5–30 μLux (less than 10^{-6} μW/cm^2), which is insufficient for adequate vision in humans (Pariente, 1980). Scotopic sensitivity is increased by the tapetum, which is a cellular structure in the mouse lemur rather than a fibrous structure as in the cat (Rohen and Castenholz, 1967; Pariente, 1970). After the first passage of light through the photoreceptor, the tapetum

serves as a mirror to allow the second passage of light. The trade-off for the increase of sensitivity is a potential decrease in resolution due to scattering of reflected light (Tansley, 1965). However, this scatter may not represent a significant factor in this species because it is the ganglion cell density that sets the limit on spatial resolution, not the density of the rods. Cone sensitivity in the mouse lemur may also benefit from tapetal reflection without an associated decrease in resolution due to the distance in spacing between adjacent cones. An additional mechanism in cones may involve the swelling observed at the junction of the inner and outer segments. For example, it has been suggested that a similar morphological feature in *Tupaia* (*ellipsoid*) increases sensitivity by channeling photons to the outer segment (Knabe et al., 1997), much like the lens-focusing effect of oil droplets in nonmammalian cones (Young and Martin, 1984). For the nocturnal mouse lemur, a gain in the sensitivity of cones could be useful during periods of dawn and dusk when light levels are in the low photopic range.

Photopigments and color vision

Our general knowledge about color vision in nocturnal primates is sparse (Dartnall et al., 1965; Bonds et al., 1987) and is limited mainly to electrophysiological data (Jacobs, 1993, 1996) because psychophysical studies are lacking. The presence of cones in nocturnal primates and the fact that they are probably not used for wavelength discrimination suggest that the function of cones differs in nocturnal and diurnal primates. The cone system of nocturnal primates may play an important role in vision during periods of dawn and dusk or for the detection of changes in irradiance in relation to circadian rhythms (Cooper et al., 1998). Indeed, behavioral observations of nocturnal primates indicate that the onset and offset of activity correspond to early dawn and late dusk periods (Pariente, 1974; Pages and Petter-Rousseaux, 1980). During these twilight periods when the animals exit or return to their nests, light levels are in the low photopic range (0.1–1 lux, 5×10^{-2} $\mu W/cm^2$) and the dominant wavelengths for reflected light are shifted toward the mid wavelength 450–500 nm region (Pariente, 1980). In addition to the mechanisms for photopic acuity and sensitivity described above, interactions between the scotopic rod system and the photopic MW cone system could provide a basis for synchronization of the circadian clock in the suprachiasmatic nucleus with environmental light/dark cycles. A role of the scant SW cone population in circadian photodetection cannot be excluded. However, the low number and irregular distribution of SW cones precludes a significant role in color vision or image formation.

ACKNOWLEDGMENTS

We thank Naura Chounlamountri for technical assistance and J. Nathans for the generous gift of antiserum. We also thank M. Perret (MNHN, Brunoy, France) for making the mouse lemurs available for this study.

LITERATURE CITED

Ahnelt PK, Kolb H. 2000. The mammalian photoreceptor mosaic-adaptive design. Prog Retin Eye Res 19:711–777.

Ahnelt PK, Hokoc JN, Röhlich P. 1995. Photoreceptors in a primitive mammal, the south american opossum, *Didelphis marsupialis aurita*: characterization with anti-opsin immunolabeling. Vis Neurosci 12: 793–804.

Blakeslee B, Jacobs GH. 1985. Color vision in the ring-tailed lemur (*Lemur catta*). Brain Behav Evol 26:154–166.

Bonds AB, Casagrande VA, Norton TT, DeBruyn EJ. 1987. Visual resolution and sensitivity in a nocturnal primate (*galago*) measured with visual evoked potentials. Vision Res 27:845–857.

Bowmaker JK, Astell S, Hunt DM, Mollon JD. 1991. Photosensitive and photostable pigments in the retinae of Old World monkeys. J Exp Biol 156:1–19.

Calderone JB, Jacobs GH. 1999. Cone receptor variations and their functional consequences in two species of hamster. Vis Neurosci 16:53–63.

Casagrande VA, DeBruyn EJ. 1982. The galago visual system: aspects of normal organization and developmental plasticity. In: Haines ED, editor. The lesser bushbaby (*Galago*) as an animal model: selected topics. Boca Raton: CRC Press. p 137–168.

Chiquet C, Dkhissi-Benyahya O, Szél A, DeGrip W, Cooper HM. 1999. Immunohistochemical characterization of calbindin positive cones in four primate species. Invest Opathalmol Vis Sci 40:S237.

Cooper HM, Kennedy H, Magnin M, Vital-Durand F. 1979. Thalamic projections to area 17 in a prosimian primate, *Microcebus murinus*. J Comp Neurol 187:145–167.

Cooper HM, Charles-Dominique P, Vienot F. 1986. Signification de la coloration des fruits en fonction de la vision des vertébrés consommateurs (Importance of fruit color for fruit-eating vertebrates). Mémoires du M.N.H.N., Série A (Zoologie) 132:131–133.

Cooper HM, Dkhissi O, Sicard B, Groscarret H. 1998. Light-evoked c-fos expression in the SCN is different under on/off and twilight conditions. In: Touitou Y, editor. Biological clocks: mechanisms and applications. p 181–188. Amsterdam: Elsevier Science.

Cserhati P, Szel A, Rohlich P. 1989. Four cone types characterized by anti-visual pigment antibodies in the pigeon retina. Invest Ophthalmol Vis Sci 30:74–81.

Curcio CA, Allen KA, Sloan KR, Lerea CL, Hurley JB, Klock IB, Milam AH. 1991. Distribution and morphology of human cone photoreceptors stained with anti-blue opsin. J Comp Neurol 312:610–624.

Dartnall HJ, Arden GB, Ikeda H, Luck CP, Rosenberg ME, Pedler CM, Tansley K. 1965. Anatomical, electrophysiological and pigmentary aspects of vision in the bush baby: an interpretative study. Vision Res 5:399–424.

DeBruyn EJ, Wise VL, Casagrande VA. 1980. The size and topographic arrangement of retinal ganglion cells in the *galago*. Vision Res 20:315–327.

Deegan JF, Jacobs GH. 1996. Spectral sensitivity and photopigments of a nocturnal prosimian, the Bushbaby (*Otolemur crassicaudatus*). Am J Primatol 40:55–66.

Dodt E. 1967. Purkinje-shift in the rod eye of the bush-baby, *Galago crassicaudatus*. Vision Res 7:509–517.

Fasick JI, Cronin TW, Hunt DM, Robinson PR. 1998. The visual pigments of the bottlenose dolphin (*Tursiops truncatus*). Vis Neurosci 15:643–651.

Goodchild AK, Ghosh KK, Martin PR. 1996. Comparison of photoreceptor spatial density and ganglion cell morphology in the retina of human, macaque monkey, cat, and the marmoset *Callithrix jacchus*. J Comp Neurol 366:55–75.

Hendrickson A, Djajadi HR, Nakamura L, Possin DE, Sajuthi D. 2000. Nocturnal tarsier retina has both short and long/medium-wavelength cones in an unusual topography. J Comp Neurol 424:718–730.

Hunt DM, Cowing JA, Patel R, Appukuttan B, Bowmaker JK, Mollon JD. 1995. Sequence and evolution of the blue cone pigment gene in Old and New World primates. Genomics 27:535–538.

Jacobs GH. 1977. Visual capacities of the owl monkey (*Aotus trivirgatus*)—I. Spectral sensitivity and color vision. Vision Res 17:811–820.

Jacobs GH. 1993. The distribution and nature of color vision among the mammals. Biol Rev 68:413–471.

Jacobs GH. 1996. Primate photopigments and primate color vision. Proc Natl Acad Sci USA 93:577–581.

Jacobs GH, Deegan JF. 1992. Cone photopigments in nocturnal and diurnal procyonids. J Comp Physiol [A] 171:351–358.

Jacobs GH, Deegan JF. 1993. Photopigments underlying color vision in Ringtail lemurs (*Lemur catta*) and Brown lemurs (*Eulemur fulvus*). Am J Primatol 30:243–256.

Jacobs GH, Deegan JF, Neitz J, Crognale MA, Neitz M. 1993. Photopig-

ments and color vision in the nocturnal monkey, *Aotus*. Vision Res 33:1773–1783.

Jacobs GH, Neitz M, Deegan JF, Neitz J. 1996a. Trichromatic color vision in New World monkeys. Nature 382:156–158.

Jacobs GH, Neitz M, Neitz J. 1996b. Mutations in S-cone pigment genes and the absence of colour vision in two species of nocturnal primate. Proc R Soc Lond [Biol] 263:705–710.

Kay RF, Kirk EC. 2000. Osteological evidence for the evolution of activity pattern and visual acuity in primates. Am J Phys Anthropol 113:235–262.

Kay RF, Ross C, Williams BA. 1997. Anthropoid origins. Science 275:797–804.

Knabe W, Skatchkov S, Kuhn HJ. 1997. "Lens mitochondria" in the retinal cones of the tree-shrew *Tupaia belangeri*. Vision Res 37:267–271.

Kremers J, Weiss S. 1997. Receptive field dimensions of lateral geniculate cells in the common marmoset (*Callithrix jacchus*). Vision Res 37: 2171–2181.

Langston A, Casagrande VA, Fox R. 1986. Spatial resolution of the Galago. Vision Res 26:791–796.

Lee BB, Smith VC, Pokorny J, Kremers J. 1997. Rod inputs to macaque ganglion cells. Vision Res 37:2813–2828.

Lythgoe JN, Partridge JC. 1989. Visual pigments and the acquisition of visual information. J Exp Biol 146:1–20.

Martin PR, Grünert U. 1999. Analysis of the short wavelength-sensitive ("blue"). Cone mosaic in the primate retina: comparison of New World and Old World monkeys. J Comp Neurol 406:1–14.

Mollon JD, Bowmaker JK. 1992. The spatial arrangement of cones in the primate fovea. Nature 360:677–679.

Muller B, Peichl L. 1989. Topography of cones and rods in the tree shrew retina. J Comp Neurol 282:581–594.

Nathans J, Thomas D, Hogness DS. 1986. Molecular genetics of human color vision: the genes encoding blue, green, and red pigments. Science 232:193–202.

Ordy JM, Samorajski T. 1968. Visual acuity and ERG-CFF in relation to the morphologic organization of the retina among diurnal and nocturnal primates. Vision Res 8:1205–1225.

Packer O, Hendrickson AE, Curcio CA. 1989. Photoreceptor topography of the retina in the adult pigtail macaque (*Macaca nemestrina*). J Comp Neurol 288:165–183.

Pages E, Petter-Rousseaux A. 1980. Annual variations in the circadian activity rhythms of five sympatric species of nocturnal prosimians in captivity. In: Charles-Dominique P, editor. Nocturnal Malagasy primates: ecology, physiology and behavior. New York: Academic Press. p 153–166.

Pariente GF. 1970. Rétinographies comparées des Lémuriens malgaches. Comparative electroretinogram of malapasy lemurs. C. R. Hebd. Séances Acad Sci 270:1404–1407.

Pariente GF. 1974. Influence of light in the activity rhythms of two Malagasy lemurs: *Phaner furcifer* and *Lepilemur mustelinus leucopus*. In: Martin RD, Doyle GA, editors. Prosimian biology. London: Duckworth. p 183–198.

Pariente GF. 1980. Quantitative and qualitative study of the light available in the natural biotope of Malagasy prosimians. In: Charles-Dominique P, editor. Nocturnal Malagasy primates: ecology, physiology and behavior. New York: Academic Press. p 117–134.

Peichl L, Moutairou K. 1998. Absence of short-wavelength sensitive cones in the retinae of seals (Carnivora) and African giant rats (Rodentia). Eur J Neurosci 10:2586–2594.

Peichl L, Wässle H. 1979. Size, scatter and coverage of ganglion cell receptive field centres in the cat retina. J Physiol 291:117–141.

Peichl L, Behrmann G, Kroger RH. 2001. For whales and seals the ocean is not blue: a visual pigment loss in marine mammals. Eur J Neurosci 13:1520–1528.

Perry VH, Oehler R, Cowey A. 1984. Retinal ganglion cells that project to the dorsal lateral geniculate nucleus in the macaque monkey. Neuroscience 12:1101–1123.

Pettigrew JD, Dreher B, Hopkins CS, McCall MJ, Brown M. 1988. Peak density and distribution of ganglion cells in the retinae of microchiropteran bats: implications for visual acuity. Brain Behav Evol 32:39–56.

Regan BC, Julliot C, Simmen B, Vienot F, Charles-Dominique P, Mollon JD. 1998. Frugivory and colour vision in *Alouatta seniculus*, a trichromatic platyrrhine monkey. Vision Res 38:3321–3327.

Rohen JW, Castenholz A. 1967. On the centralization of the retina in primates. Folia Primatol 5:92–147.

Röhlich P, Szel A. 1993. Binding sites of photoreceptor-specific antibodies COS-1, OS-2 and AO. Curr Eye Res 12:935–944.

Sandmann D, Boycott BB, Peichl L. 1996. Blue-cone horizontal cells in the retinae of horses and other equidae. J Neurosci 16:3381–3396.

Stone J, Johnston E. 1981. The topography of primate retina: a study of the human, bushbaby, and new- and old-world monkeys. J Comp Neurol 196:205–223.

Szel A, Röhlich P. 1992. Two cone types of rat retina detected by anti-visual pigment antibodies. Exp Eye Res 55:47–52.

Szel A, Takacs L, Monostori E, Diamantstein T, Vigh-Teichmann I, Röhlich P. 1986. Monoclonal antibody-recognizing cone visual pigment. Exp Eye Res 43:871–883.

Szel A, Diamantstein T, Röhlich P. 1988. Identification of the blue-sensitive cones in the mammalian retina by an anti-visual pigment antibody. J Comp Neurol 273:593–602.

Szel A, Röhlich P, Caffe AR, Juliusson B, Aguirre G, Van Veen T. 1992. Unique topographic separation of two spectral classes of cones in the mouse retina. J Comp Neurol 325:327–342.

Szel A, Röhlich P, Caffe AR, van Veen T. 1996. Distribution of cone photoreceptors in the mammalian retina. Microsc Res Tech 35:445–462.

Szel A, Lukats A, Fekete T, Szepessy Z, Röhlich P. 2000. Photoreceptor distribution in the retinas of subprimate mammals. J Opt Soc Am [A] 17:568–579.

Tan Y, Li WH. 1999. Trichromatic vision in prosimians. Nature 402:36.

Tansley K. 1965. Vision in vertebrates. London: Cox and Wyman.

Treff H. 1967. Tiefensehschärfe und Sehschärfe beim Galago (*Galago senegalensis*). Z vergleichende Physiol 54:26–57.

Vissers PM, DeGrip WJ. 1996. Functional expression of human cone pigments using recombinant baculovirus: compatibility with histidine tagging and evidence for N- glycosylation. FEBS Lett 396:26–30.

von Schantz M, Argamaso-Hernan SM, Szel A, Foster RG. 1997. Photopigments and photoentrainment in the Syrian golden hamster. Brain Res 770:131–138.

Wang Y, Macke JP, Merbs SL, Zack DJ, Klaunberg B, Bennett J, Gearhart J, Nathans J. 1992. A locus control region adjacent to the human red and green visual pigment genes. Neuron 9:429–440.

Wässle H, Boycott BB. 1991. Functionnal architecture of the mammalian retina. Physiol Rev 71:447–480.

Wikler KC, Rakic P. 1990. Distribution of photoreceptor subtypes in the retina of diurnal and nocturnal primates. J Neurosci 10:3390–3401.

Yamada ES, Marshak DW, Silveira LC, Casagrande VA. 1998. Morphology of P and M retinal ganglion cells of the bush baby. Vision Res 38:3345–3352.

Yamada ES, Silveira LC, Perry VH, Franco EC. 2001. M and P retinal ganglion cells of the owl monkey: morphology, size and photoreceptor convergence. Vision Res 41:119–131.

Yokoyama S, Yokoyama R. 1989. Molecular evolution of human visual pigment genes. Mol Biol Evol 6:186–197.

Young SR, Martin GR. 1984. Optics of retinal oil droplets: a model of light collection and polarization detection in the avian retina. Vision Res 24:129–137.